3
Characterization of Solid Catalysts

3.1
Physical Properties

3.1.1
Surface Area and Porosity

Alexander V. Neimark, Kenneth S. W. Sing, and Matthias Thommes*

3.1.1.1 Introduction

Most catalysts of practical importance are highly porous and possess large specific surface areas. Although the catalytic activity may be only indirectly related to the total available surface, evaluation of the surface area is generally considered to be an important requirement in catalyst characterization [1, 2]. In addition, it is necessary to assess the pore size distribution in order to investigate whether the molecular transportation and reaction pathways are affected by changes in the pore structure.

Before we discuss the various procedures that are currently employed for determining the surface area and pore size distribution, it is necessary to define the various terms commonly associated with the properties of porous catalysts. The definitions in Table 1 are consistent with those proposed by IUPAC [3] and other official organizations [4]. As indicated, the pore size is generally specified as the internal pore width, w, although in the context of capillary condensation [5–7] it has been customary to refer to the pore radius, r_p. Of course, such terms have a precise meaning only when the pore shape is properly defined. Furthermore, the internal or effective pore width must not be confused with the distance between the centers of surface atoms, which is usually employed in simulation work (i.e. the outer atoms of solid in the opposite walls of a pore). A regular cylindrical pore shape was originally assumed [5], but over the past 50 years various other more realistic pore shapes have been introduced [5–7], such as uniform slits (e.g. in activated carbons and clays), ink-bottle pores (e.g. in porous glass) and interstices between globular particles (e.g. in porous silicas). Recent advances have included the application of fractal geometry [8] and the statistical modeling of disordered pore networks [9].

It has become fashionable to refer to micropores and mesopores as ''nanopores''. The upper limit of the nanopore dimensions is somewhat arbitrary, but there is a certain advantage in adopting this flexible approach since it allows us to focus attention on the overall behavior of a nanoporous material rather than on any fixed scale of pore size. Similarly, it is expedient to refer to narrow micropores (of $w < 1$ nm) as ultramicropores and to wider micropores (of 1 nm $< w < 2$ nm) as supermicropores, although it should be understood that the process of pore filling is dependent on, *inter alia*, the ratio w/d (d being the molecular diameter).

It is not always easy to distinguish between roughness and porosity. In principle, a simple convention is to refer to a solid as porous if the surface irregularities are deeper than they are wide. It is also convenient to regard the area of a rough or macropore surface as the *external* surface area and the area of the micropore or mesopore walls as the *internal* area.

It must be kept in mind that the recorded values of surface area, porosity, pore size and pore volume are likely to depend on the experimental methods used. In the case of a highly porous catalyst, no experimental technique should be expected to provide absolute values of these parameters and the choice of a particular procedure should take into consideration the nature of the catalyst or support and its application. Since methods are most often used to determine the effective (or apparent) surface area and pore size distribution, most attention must be given to these procedures. However, the principles and application of some other

* Corresponding author.

References see page 736

Handbook of Heterogeneous Catalysis, 2nd Ed.
Edited by G. Ertl, H. Knözinger, F. Schüth, and J. Weitkamp

ISBN: 978-3-527-31241-2

Tab. 1 Some definitions associated with porous solids

Term	*Definition*
Porous solid	Solid with cavities or channels that are deeper than they are wide
Open pore	Cavity or channel with access to the surface
Interconnected pore	Pore that communicates with other pores
Blind pore[a]	Pore with a single connection to the surface
Closed pore	Cavity not connected to the surface
Void	Space between particles
Micropore	Pore of internal width less than 2 nm
Mesopore	Pore of internal width between 2 and 50 nm
Macropore	Pore of internal width greater than 50 nm
Pore size	Pore width – diameter or distance between opposite walls
Pore volume	Volume of pores determined by a stated method
Porosity	Ratio of pore volume to overall volume of particle or granule
Surface area	Area of total surface, as determined by stated method
Internal surface area	Area of pore walls
External surface area	Area of surface outside micropores and mesopores
True density	Density of solid, excluding pores and voids
Apparent density	Density of solid including pores, as determined by stated method
Tortuosity	Ratio of path available for diffusion to distance across porous bed
Zeolitic cage	Intracrystalline pore with windows allowing no passage of molecules larger than H_2O
Zeolitic channel	Intracrystalline pore extending infinitely in one direction allowing passage of molecules

[a] Also called a ''dead-end pore''.

methods are discussed briefly in Sections 3.1.1.3 and 3.1.1.4.

3.1.1.2 Physisorption of Gases

Physisorption (physical adsorption) is a general interfacial phenomenon and, unlike chemisorption, occurs whenever a gas (the *adsorptive*) is brought into contact with the surface of a solid (the *adsorbent*). The matter in the adsorbed state is known as the *adsorbate*, as distinct from the adsorptive, which is the adsorbable gas.

The forces involved in physisorption are the same as those responsible for the condensation of vapors and the deviations from ideal gas behavior. They always include the long-range London dispersion forces and the short-range intermolecular repulsion. These combined forces give rise to *non-specific* molecular interactions. Various types of *specific* interactions come into play when polar molecules are adsorbed on ionic or polar surfaces, but the process is still regarded as physisorption unless there is some form of chemical bonding.

The amount, n, of gas adsorbed by unit mass of the adsorbent is dependent on the equilibrium pressure p, the temperature T and the nature of the gas–solid system. Thus, we may write

$$n = \mathrm{f}(p, T, system) \tag{1}$$

If the particular gas is below its critical temperature and the adsorbent is maintained at a constant temperature, the adsorption isotherm for the given gas–solid system is

$$n = \mathrm{f}\left(\frac{p}{p^0}\right)_T \tag{2}$$

where p^0 is the saturation pressure of the adsorptive at T. The *adsorption isotherm* is thus the relationship, usually presented in graphical form, between the amount adsorbed and the equilibrium pressure or relative pressure, at the known temperature.

The first step in the interpretation of a physisorption isotherm is inspection of its shape. The classification of physisorption isotherms and associated hysteresis loops shown in Fig. 1 was proposed by IUPAC [10]. It still provides a starting point for identifying the adsorption and pore filling mechanisms and thus deciding which computational procedures are most likely to yield useful quantitative information.

Reversible Type I isotherms are given by microporous adsorbents such as zeolites and many activated carbons. The limiting uptake at the plateau is mainly dependent on the accessible micropore volume rather than on the internal surface area. Thus, if the plateau is almost flat, multilayer adsorption is only possible on a small external surface. A steep uptake at very low p/p^0 is due to enhanced adsorbent–adsorbate interactions in

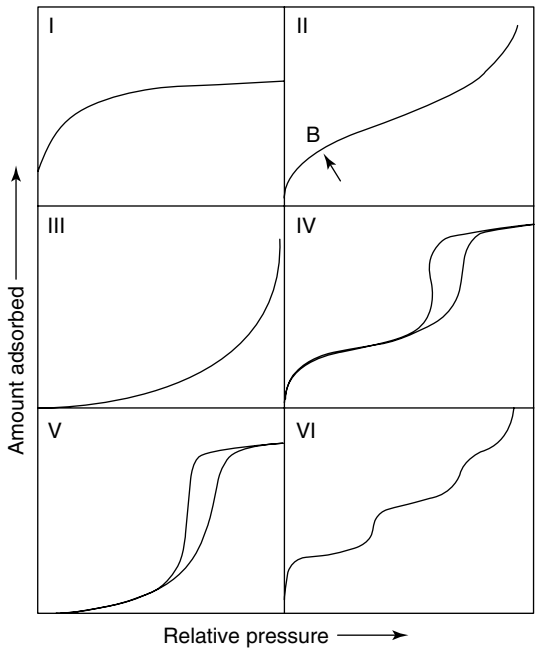

Fig. 1 Types of physisorption isotherms.

ultramicropores (micropores of molecular dimensions), resulting in micropore filling at very low p/p^0. Some composite isotherms appear to have Type I character while also exhibiting H4 hysteresis loops (types of hysteresis loops are shown in Fig. 3). Such behavior is generally associated with a wide range of narrow slit-like nanopores.

Reversible Type II isotherms are given by the physisorption of gases on most non-porous or macroporous adsorbents. The shape is the result of unrestricted monolayer–multilayer adsorption up to high p/p^0. If the knee is sharp, point B – the beginning of the middle almost linear section – usually corresponds to the completion of monolayer coverage. A more gradual curvature (i.e. a less distinctive point B) is an indication of a significant amount of overlap of monolayer coverage and the onset of multilayer adsorption. In the extreme case of a Type III isotherm, there is no point B and therefore no identifiable monolayer; the adsorbent–adsorbate interactions are now relatively weak and the adsorbed molecules are clustered around the most favorable sites.

The non-reversibility of a pseudo-Type II isotherm is manifested in the form of the H3 hysteresis loop. The shape of the adsorption branch appears to indicate normal monolayer–multilayer adsorption since there is no limiting adsorption at high p/p^0, but this may be misleading. Such isotherms are often observed with aggregates of plate-like particles (e.g. clays) giving rise to assemblages of non-rigid slit-shaped pores.

Type IV isotherms are given by mesoporous adsorbents (e.g. many oxide gels). In this case, the initial monolayer–multilayer adsorption on the mesopore walls is followed by capillary condensation. A characteristic feature of most Type IV isotherms is the appearance of H1 or H2 hysteresis loops (see Fig. 3). The H1 loop is indicative of a narrow range of uniform mesopores, whereas the more common H2 loop can usually be attributed to percolation effects in a complex pore network and cavitation effects in ink-bottle pores [11, 12]. Some ordered mesopore structures (notably MCM-41 with pores narrower than ~4 nm) give completely reversible Type IV isotherms [6], which were not known at the time of the original IUPAC classification [10].

In the low p/p^0 range, the Type V isotherm shape is similar to that of Type III and can be attributed to relatively weak adsorbent–adsorbate interactions. At higher p/p^0, molecular clustering is followed by nanopore filling. Type V water isotherms are given by some activated carbons, but are otherwise uncommon.

The stepwise Type VI isotherm is representative of layer-by-layer adsorption on a highly uniform surface. The step height now represents the capacity for each adsorbed layer, whereas the sharpness of the step is dependent on the system and the temperature. Amongst the best examples of Type VI isotherms are those obtained with argon or krypton at low temperature on graphitized carbon blacks.

The experimental procedures used for determining the amount of gas adsorbed are either those that depend on measurement of the gas removed from the gas phase (i.e. volumetric or manometric methods) or those that involve the direct measurement of the change in mass of the adsorbent (i.e. gravimetric methods). In recent years, automated adsorption equipment has been installed in almost every organization concerned with the production or characterization of catalysts. The development of excellent commercial equipment has been accompanied by the installation of user-friendly software, but there has been a tendency to overlook some of the fundamental principles involved in the interpretation of the isotherm data. It is therefore appropriate to examine in some detail the scope and limitations of the physisorption as a means of determining the surface area and porosity of catalysts.

3.1.1.2.1 Determination of Surface Area

A The BET Method In spite of its theoretical limitations [5–7], the Brunauer–Emmett–Teller (BET) method [13] continues to be widely used for evaluating the surface area of catalysts and supports. It is now generally agreed that the BET theory was based on an oversimplified model of physisorption. As a consequence, the BET method is applied in an empirical manner and

References see page 736

therefore it is necessary to ensure that certain conditions are fulfilled before the ''BET area'' can be accepted as a meaningful surface area [5, 6]. Two stages are involved in the evaluation of the BET area. First, it is necessary to transform a physisorption isotherm into the ''BET plot'' and from it to derive the value of the BET monolayer capacity, n_m. The second stage is the calculation of the specific surface area, a_{BET}, which requires a knowledge of the molecular area, σ.

In its original form, the BET theory [13] was essentially a multilayer extension of Langmuir's kinetic treatment of monolayer adsorption on an array of identical sites. Thus, the Langmuir concept of the *ideal localized* monolayer was extended to include the formation of either an infinite or a finite number of adsorbed layers. The molecules in the first layer were assumed to act as sites for the second-layer molecules, which in turn provide sites for the adsorption of molecules in the higher layers. Equilibration is attained at a given temperature when the rate of condensation (i.e. adsorption) is equal to the rate of evaporation (i.e. desorption). For the steady-state adsorption in each layer we therefore have an equation of the form

$$a_i p\theta_{i-1} = b_i\theta_i \exp\left(\frac{-E_i}{RT}\right) \tag{3}$$

where θ_{i-1} and θ_i represent the fractions of surface covered by the $i-1$th and ith layers, respectively, a_i and b_i are adsorption and desorption constants and E_i is the energy of adsorption for the ith layer. In principle, each layer has a different set of values of a_i, b_i and E_i, but in order to simplify the summation of the amounts adsorbed, it was necessary to assume that for all layers after the first, these parameters remain constant and that $E_i = E_L$, the liquefaction energy.

With the further assumption that the multilayer has an infinite thickness at $p/p^0 = 1$, it was possible to arrive at the well-known BET equation, which is usually expressed in the following linear form:

$$\frac{\left(\frac{p}{p^0}\right)}{\left[n\left(\frac{1-p}{p^0}\right)\right]} = \left(\frac{1}{n_m C}\right) + \left[\frac{(C-1)}{n_m C}\right]\left(\frac{p}{p^0}\right) \tag{4}$$

where n_m is the monolayer capacity and C is an empirical constant.

According to the original theory, the parameter C is related exponentially to E_i by the equation

$$C = \exp\left[\frac{(E_1 - E_L)}{RT}\right] \tag{5}$$

The quantity $(E_1 - E_L)$ was originally known as the ''net heat of adsorption''. Although Eq. (5) must now be regarded as an oversimplification [5], the value of C does appear to give an indication of the order of magnitude of the adsorbent–adsorbate interactions.

According to Eq. (4), n_m and C can be easily calculated from the slope and intercept of the linear BET plot of $p/n(p^0 - p)$ versus p/p^0. In practice, the range of linearity of the BET plot is always restricted to a limited part of the isotherm [2, 5, 6]. Linearity is rarely found outside the p/p^0 range 0.05–0.30 and with a few systems (e.g. argon or nitrogen at 77 K on graphitized carbon) the upper limit is not above $p/p^0 \approx 0.10$. Some physisorption systems appear to give linear BET plots over several ranges of p/p^0, but it is only in the region of point B that the BET plot can be expected to yield the required value of n_m.

If C > 2, the mathematical form of Eq. (4) is similar to that of the Type II isotherm in Fig. 1. This has been called the S-shaped, or sigmoid, isotherm. However, if $C < 2$, the shape is changed and the point of inflection is lost. The BET equation then gives a Type III isotherm (see Fig. 1). A high value of C (at least ~100) is associated with a fairly sharp knee and then n_m and the uptake at point B are in fairly close agreement (generally to within a few percent). In this case, point B can be identified by visual inspection, although it is not possible to give a precise mathematical description of its location.

With some systems, the range of fit can be improved by restricting the number of layers to N at $p/p^0 = 1$, thus giving an extended form of the BET equation [13]. In the special case of $N = 1$, as expected, this extended BET equation is reduced to the simple Langmuir form of equation for ideal localized monolayer adsorption. It is also of particular interest [4] that if $N > 5$, the deviation from Eq. (4) becomes significant only above $p/p^0 \approx 0.5$, which is well outside the normal BET range.

An alternative and more elegant derivation of the BET equation is obtained by a statistical mechanical treatment [14]. As before, all the surface sites are identical and now the occupation probability of a particular site is assumed to be independent of the occupancy of neighboring sites. Also, the probability of the occupation of a multilayer site is taken as zero unless all its underlying sites are already occupied. Furthermore, it is assumed that the partition functions for the second and higher layers are the same as for molecules in the liquid state. This treatment gives an isotherm equation of the same general form as the BET equation, but the parameter C is now defined in terms of the ratio of the partition functions for molecules in the first layer and in the liquid state.

In spite of the statistical mechanical refinement, the BET model is still unrealistic in a number of important respects. The notion of localized adsorption on an array of equivalent sites implies no variation in the energy of adsorption over the complete range of monolayer coverage. In fact, adsorption calorimetry has

revealed [6] that most adsorbents exhibit a high degree of energetic heterogeneity. Generally, the differential energy of adsorption undergoes a marked decrease – especially at low fractional coverage – as the monolayer population is increased [6]. Although this behavior is incompatible with the BET model, the range of linearity of the BET plot tends to be somewhat more extensive than is found with a more homogeneous surface such as graphitized carbon [5]. In the latter case, the adsorbate–adsorbate interactions can often be detected long before monolayer coverage is complete – again in disagreement with the requirements of the BET model.

In the light of these findings, it is necessary to examine the experimental evidence for the significance of point B and hence the validity of n_m. Powerful evidence has been provided by the calorimetric determination of adsorption energy data [5, 6]. With some adsorption systems, a sharp decrease in the differential energy of adsorption has been observed in the vicinity of point B [5]. When this is preceded by increased adsorption energy at high surface coverage, we may conclude that there are fairly strong molecular interactions within the densely packed monolayer. In contrast, a monotonous decline in the adsorption energy over the whole range of monolayer coverage is consistent with the more typical surface heterogeneity [6].

As already indicated, we obtain the specific surface area, a_{BET}, from n_m by assuming a value for the area, σ, occupied by each adsorbate molecule (i.e. the effective molecular cross-sectional area) in the completed monolayer. Thus,

$$a_{BET} = n_m L \sigma \tag{6}$$

where L is the Avogadro constant.

For a number of reasons [5–7], nitrogen (at 77 K) is generally considered to be the most suitable adsorptive for the determination of the surface area of non-porous, macroporous or mesoporous solids. Following the early work of Emmett and Brunauer [15], it is usually assumed that the nitrogen monolayer is close-packed as in its liquid state at 77 K, thus giving $\sigma_N = 0.162\ nm^2$. With this value inserted into Eq. (6), it is therefore possible to evaluate the BET-nitrogen area from n_m. However, since the nitrogen–surface interactions are dependent on the adsorbent structure [5, 6], some variation in σ_N is to be expected. As already pointed out, an additional problem is the heterogeneous nature of many surfaces, which, of course, include supported and other multicomponent catalysts. Unfortunately, it is not easy to obtain completely independent verification of BET-nitrogen areas. Comparisons [5, 6, 16] made between the derived values of $a_{(BET,N_2)}$ and independently determined areas (e.g. geometric areas determined by electron microscopy) are somewhat inconclusive, but indicate that it is possible to obtain agreement within ~20%.

Argon may seem to be an alternative adsorptive for surface area determination. Its molecule is monatomic and much less reactive than the diatomic nitrogen molecule. To obtain the BET-argon area, $a_{(BET,Ar)}$, the molecular area of argon at 77 K was originally taken as $0.138\ nm^2$ [13, 15]. The many comparisons made between the surface areas determined by argon and nitrogen adsorption [5–7, 16] have revealed that the corresponding derived values of $a_{(BET,Ar)}$ and $a_{(BET,N_2)}$ cannot be brought into agreement unless *ad hoc* adjustments are made in the apparent molecular areas of either argon or nitrogen. There are, however, several reasons why argon at 77 K is considered to be less reliable than nitrogen [5, 6]. At 77 K, all nitrogen isotherms on non-porous adsorbents are Type II, whereas some argon isotherms are Type II and others are Type VI. These and other differences indicate that at 77 K, the structure of the argon monolayer is highly dependent on the surface chemistry of the adsorbent.

An alternative is argon adsorption at 87 K, i.e. at liquid argon temperature. Here, the problems discussed for argon adsorption at 77 K are not present. A cross-sectional area, σ_{Ar}, of $0.142\ nm^2$ is usually assumed. Because of the absence of a quadrupole moment and the higher temperature, σ_{Ar} is less sensitive to differences in structure of the adsorbent surface [5]. Furthermore, argon adsorption at 87 K offers advantages for both micropore and mesopore analysis (see Section 3.1.1.2.1B).

With other adsorptives, empirical adjustment of σ is similarly required if one attempts to bring the derived a_{BET} values into agreement with the corresponding BET-nitrogen areas [5, 6, 16]. In some cases (e.g. carbon dioxide and polar organic molecules) there are strong specific interactions with ionic or polar surfaces [5, 6] so that the BET C values may vary considerably from one surface to another. A relatively low value of C (say, $C < 80$) is indicative of a significant overlap of monolayer and multilayer adsorption and consequently of an increased level of uncertainty in the reliability of n_m.

The ready availability of liquid nitrogen and present-day reliability of user-friendly commercial equipment make it relatively easy to determine nitrogen isotherms at 77 K. Also because of this, nitrogen has become the standard BET adsorptive with the convention that $\sigma_N = 0.162\ nm^2$ [15, 17]. Hence for routine work, it is assumed that the BET monolayer is in the close-packed "liquid" state, irrespective of the actual structure of the completed monolayer. However, for some materials (e.g. materials with polar surfaces), the accuracy of the BET analysis can be improved by using argon as the adsorptive at the liquid argon temperature of 87 K.

References see page 736

For operational reasons, it becomes difficult to measure the adsorption of nitrogen if the specific surface area is relatively low (i.e. if $a < 2\ m^2\ g^{-1}$). In this event, krypton adsorption at 77 K can be used to minimize the dead space correction and hence improve the accuracy in measuring the small amounts adsorbed. This is the benefit gained by using a gas with a low saturation pressure at 77 K. On the other hand, there remains the problem of selecting the "best" value of σ_{Kr} for the particular adsorbent [3, 5].

The determination of the surface area of an ultramicroporous catalyst (e.g. a molecular sieve zeolite) presents a major problem. Since monolayer–multilayer adsorption cannot take place in pores of molecular dimensions, the BET method is strictly not applicable. Although BET areas are often quoted in the scientific or commercial literature, they should be regarded as "apparent areas". They are sometimes recorded as part of the characterization "fingerprint" of a catalyst, which may be useful in a patent specification, but they have little value in fundamental research.

B The Standard Isotherm Concept Various attempts have been made to express physisorption isotherm data in a standard form [5]. One way of normalizing an isotherm is to plot it in the dimensionless, reduced form of the statistical number, n/n_m, of adsorbed molecular layers against p/p^0. This is a simple way of comparing the isotherms of a particular adsorptive on different adsorbents. For example, the approach was used many years ago [18, 19] to demonstrate that *multilayer* nitrogen isotherms on a wide range of non-porous solids could be represented fairly well by a common Type II curve.

The reduced adsorption can be converted into the statistical thickness, t, of the adsorbed layer by the relation

$$t = \left(\frac{n}{n_m}\right) d^* \tag{7}$$

where d^* is now the effective thickness of each molecular layer. Following the work of Lippens and de Boer [20], it is usually assumed that the density of the adsorbate is the same as that of the liquid adsorptive at the operational temperature. Thus, in the case of nitrogen adsorption at 77 K, the notional multilayer thickness becomes

$$t = \frac{0.354n}{n_m}(\text{nm}) \tag{8}$$

The fact that many nitrogen isotherms can be superposed in the *multilayer* range has important implications for both surface area determination and pore size analysis, but the claim by de Boer [21] that this provided a "universal multilayer thickness curve" for nitrogen adsorption is now regarded as an oversimplification [6]. Moreover, the approach suffers from the disadvantage that the validity of n_m is assumed.

An alternative, and simpler, approach is to express the normalized adsorption as n/n_x, where n_x is the amount adsorbed at a preselected standard p/p^0 [22]. This procedure has the advantage that it is independent of the BET method. The choice of the standard p/p^0 is to some extent arbitrary, but with the isotherms of a number of different adsorptives it has been found convenient to place $n/n_x = \alpha_S = 1$ at $p/p^0 = 0.4$ [22]. The standard isotherm for a given adsorptive on a non-porous reference material is thus set up in the form of α_S versus p/p^0. The characteristic features of another isotherm can now be quantitatively analyzed by the construction of the α_S plot of n against α_S [5, 6, 22].

Provided that certain conditions are fulfilled [5, 6], it is possible to use the α_S method to (i) identify the physisorption mechanisms, (ii) check the validity of the BET-nitrogen area, (iii) evaluate the total surface area of a non-porous or mesoporous solid and (iv) assess the effective micropore volume and external area of an ultramicroporous or supermicroporous solid. The application of the α_S method is discussed in more detail in relation to the assessment of microporosity.

3.1.1.2.2 Assessment of Porosity

A Capillary Condensation and the Kelvin Equation The sorption behavior in mesopores is determined not only by the adsorption potential (i.e. the fluid–wall interactions), but also by the attractive interactions between the fluid molecules. As a consequence, one can observe, in addition to multilayer adsorption, pore condensation. Pore condensation is the phenomenon whereby a gas condenses to a liquid-like phase in a pore at a pressure p less than the saturation pressure p^0 of the bulk liquid. This leads to the appearance of a Type IV adsorption isotherm in the IUPAC classification (see Fig. 1).

It is interesting that the first section of the Type IV isotherm is identical with the corresponding isotherm given by a chemically similar non-porous solid (i.e. of Type II) having the same surface area. This means that the monolayer coverage and the initial stages of multilayer adsorption occur on the mesopore walls in the same manner as on the open surface. However, at a certain p/p^0 the Type IV isotherm can be seen to deviate away from the corresponding Type II isotherm. This upward swing is now associated with the filling of the mesopores by capillary condensation. Its occurrence at a pressure (which depends on the pore size) below the normal saturation pressure is due to the formation of a curved meniscus in a group of pores of particular size and shape. If one assumes complete wetting behavior of the pore condensate, the equation which relates the curvature

of the liquid meniscus in a pore to the relative pressure at which condensation occurs is [3, 5]

$$\frac{1}{r_1} + \frac{1}{r_2} = -\frac{RT}{\gamma v_l} \ln\left(\frac{p}{p^0}\right) \tag{9}$$

where r_1 and r_2 are the principal radii of curvature, γ is the surface tension of the liquid condensate and v_l is its molar volume (note that in case of nitrogen and argon sorption at 77 and 87 K, respectively, the vapor density is so small that it can be neglected). Rearrangement of Eq. (9) and replacement of $1/r_1 + 1/r_2$ by $2/r_k$ gives the more familiar form of the Kelvin equation:

$$r_k = -\frac{2\gamma v_l}{RT} \ln\left(\frac{p}{p^0}\right) \tag{10}$$

in which r_k is often referred to as the Kelvin radius. Clearly, r_k would represent the radius of curvature of a hemispherical meniscus (since $r_1 = r_2 = r_k$). If the pores are in the form of parallel-sided slits, $r_2 = \infty$ and the meniscus is cylindrical.

In case of complete wetting, the pore walls are covered by a multilayer adsorbed film at the onset of pore condensation and the thickness t of this multilayer film has to be taken into account in any calculation of the pore radius or width of the group of mesopores. Thus, for cylindrical pores, the pore radius r_p is given by

$$r_p = r_k + t \tag{11}$$

and, for parallel-sided slits, the width w_p is given by

$$w_p = r_k + 2t \tag{12}$$

The modified Kelvin equation based on a cylindrical pore model [Eq. (11)] serves as the basis for many methods applied for mesopore analysis, including the Barrett–Joyner–Halenda (BJH) method [23], which is still widely used. This procedure is based on the notional emptying of the pores by a stepwise reduction of p/p^0 by taking into account the thinning of the multilayer in those pores already emptied of the condensate. The derived mesopore size distribution is usually expressed in a graphical form, for example, $\Delta V_p/\Delta r_p$ vs. r_p. In order to account for the preadsorbed multilayer film, the Kelvin equation is combined with a standard isotherm (the so-called t-curve), which has been determined on a number of well-defined non-porous solids. However, with narrow pores (if $w_p < \sim 10$ nm) the standard t-curve does not correspond exactly with the real thickness of the preadsorbed multilayer film, because curvature effects and surface forces are not taken into account.

The validity of the Kelvin equation also becomes questionable because it does not allow for the effect of the adsorption forces on the pore condensation. Furthermore, the macroscopic, thermodynamic concept of a smooth liquid–vapor interface and bulk-like core fluid cannot be realistically applied to condensation in narrow mesopores. It is evident that the Kelvin concept fails to describe correctly the peculiarities of the critical region and the confinement-induced shifts of the phase diagram of the pore fluid and the hysteresis behavior (for reviews, see Refs. [7] and [24]).

Direct experimental tests of the validity of the Kelvin equation were made possible by the development of model mesoporous silicas (the so-called M41S materials, SBA-15, etc.) over the past decade (for a review, see Ref. [7]). The most prominent representative of these materials is MCM-41, which consists of an array of independent cylindrical pores (of the same diameter in the range 2–10 nm). Because of the high degree of order, the pore diameter can be derived by independent methods [based on X-ray diffraction (XRD), high-resolution transmission electron microscopy, etc.]. It is found that the BJH method and related procedures based on a modified Kelvin equation (e.g. the Broekhoff–de Boer method) can underestimate the pore size by up to 20–30% for pores smaller than 10 nm. An improvement can be achieved by *calibrating* the Kelvin equation using a series of MCM-silicas of known pore diameter (obtained from XRD interplanar spacing and the mesopore volume). In this manner, a relation between capillary condensation pressures and pore size can be established and used to obtain an empirically corrected Kelvin equation (which is the basis of the so-called Kruk–Jaroniec–Sayari method) over the calibrated range (i.e. 2–7 nm) [25].

B Adsorption Hysteresis A physisorption hysteresis loop is generally dependent on two phenomena: adsorption–desorption within a single pore of given shape and effects related to the pore network connectivity. On the pore level, the hysteresis can be regarded as an intrinsic property of the vapor–liquid phase transition in a finite volume system. A classical scenario of capillary condensation implies that the vapor–liquid transition is delayed due to the existence of metastable adsorption films and hindered nucleation of liquid bridges [26–28]. In principle, both condensation and evaporation can be associated with metastable states of the pore fluid.This is consistent with the classical van der Waals theory, which predicts that the metastable adsorption branch terminates at a vapor-like spinodal that corresponds to the limit of stability for the metastable adsorbed films. Similarly, the metastable desorption branch terminates at a liquid-like spinodal, which corresponds to the limit of stability of metastable (stretched) condensed fluid. In open uniform

References see page 736

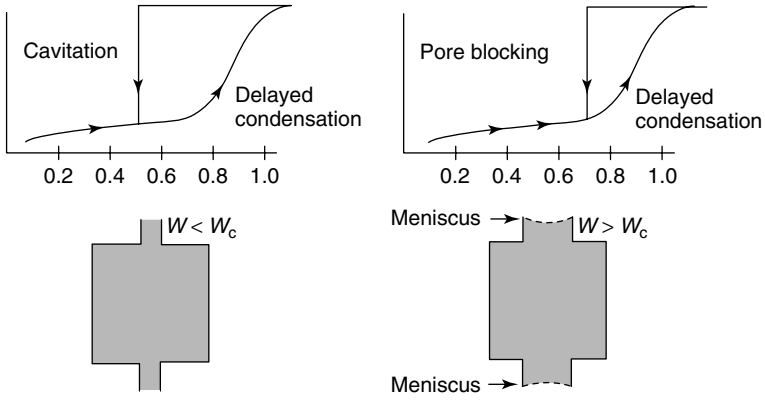

Fig. 2 Schematic illustration of pore blocking and cavitation phenomena (after Ref. [12a]).

cylindrical pores of finite length, however, metastabilities occur only on the adsorption branch. Indeed, in an open pore filled by liquid-like condensate, the liquid–vapor interface is already present and evaporation therefore occurs without nucleation, via a receding meniscus. That is, the desorption process is associated with the equilibrium vapor–liquid transition, whereas the condensation process involves nucleation of liquid bridges. In sufficiently wide pores, the barrier in the nucleation process is so high that condensation is delayed and occurs spontaneously close to the vapor-like spinodal.

In order to describe hysteresis phenomena in disordered pore structures, network models have been developed (e.g. [29–32]). The network models attribute hysteresis to the so-called *pore blocking* or *percolation* effect. This effect is expected to occur if a pore has access to the external surface only through a narrower neck, as in an ink-bottle pore. The wide body of an ink-bottle pore is filled at the vapor pressure, which corresponds to the delayed condensation and remains filled during desorption until the narrow neck empties first at a lower vapor pressure. Thus, in a network of ink-bottle pores, evaporation of the capillary condensate is obstructed by the pore necks. The vapor pressure at which a pore body empties depends on the size of the necks, the connectivity of the network and the state of the neighboring pores. The pore network empties when the relative pressure is below a characteristic *percolation* threshold associated with the onset of a continuous cluster of pores open to the surface.

Adsorption–desorption mechanisms were recently revisited with the aid of model materials, which contained well-defined ink-bottle pores, [11, 12, 33–35]. The theoretical and experimental studies have revealed that if the neck diameter is smaller than a critical size (estimated to be ca. 5 nm for nitrogen at 77 K), the mechanism of desorption from the larger region involves cavitation (i.e. the spontaneous nucleation of gas bubbles). Thus, for a given adsorptive and temperature, the neck diameter of an ink-bottle pore determines the mechanism of evaporation from the pore body. This situation is illustrated schematically in Fig. 2. In the case of pore blocking in a neck of diameter larger than the critical size, evaporation occurs at the equilibrium pressure of the corresponding meniscus and therefore information about the neck size can be obtained from the desorption branch of the isotherm. In the case of a smaller neck, the cavitation takes place and the evaporation pressure is not related to the neck size and therefore no information about the neck width can be obtained from the analysis of the desorption branch.

The shape of the hysteresis loop reflects the specifics of texture (e.g. pore size distribution, pore geometry, connectivity) of a mesoporous adsorbent.

An empirical classification of hysteresis loops was given by IUPAC [10], which is shown in Fig. 3. According to the IUPAC classification, type H1 is often associated with porous materials exhibiting a narrow distribution of relatively uniform (cylindrical-like) pores. In principle, an H1 hysteresis loop is mainly determined by the effect of delayed condensation and not by network effects. It follows that the desorption branch can be used for pore size analysis. Materials that give rise to H2 hysteresis contain a more complex pore structure in which network effects are important. In this case, any simple analysis of the desorption branch is likely to give a misleading picture of the pore size and it is recommended that the pore size distribution should be calculated from the adsorption branch – if possible, with allowance made for delayed condensation. Isotherms with type H3 hysteresis do not exhibit any limiting adsorption at high p/p^0. They are given by non-rigid aggregates of plate-like particles or assemblages of slit-shaped pores and in principle should not be expected to provide a reliable assessment of either the pore size distribution or the total pore volume. H4 hysteresis loops are generally observed with complex materials containing both micropores and mesopores.

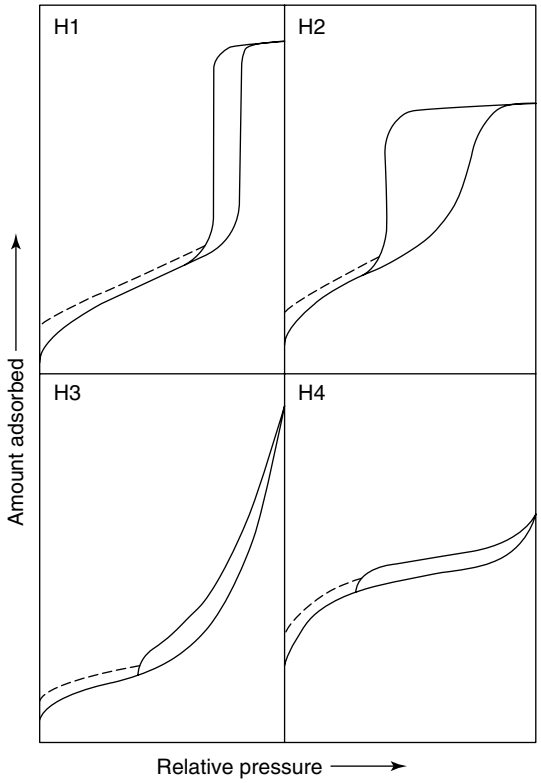

Fig. 3 Types of hysteresis loops.

A particular feature of many H2, H3 and H4 hysteresis loops is a very steep region of the desorption branch. This is often associated with a lower closure point of the loop at an almost constant p/p^0 for a given adsorptive and temperature (e.g. $p/p^0 = 0.42$ for nitrogen at 77 K and 0.38 for argon at 87 K). This characteristic step-down is dependent on the properties of the adsorptive (i.e. instability of the condensate due to cavitation) rather than with the evaporation of pore fluid from a certain class of pores [5]. Hence the calculations from the desorption branch may lead to an artificial narrow peak in the pore size distribution.

Recently, advanced methods based on density functional theory (DFT) have been developed for pore size analysis (e.g. [36, 37]), which take into account the particular features of the hysteresis.

C Microporosity In the IUPAC classification of pore sizes [10], the upper limit of the micropore width is placed at about 2 nm. This limiting width is necessarily somewhat arbitrary, since the mechanism of pore filling is controlled by the pore dimensions and also by the size of the adsorptive molecules and their interactions with the adsorbent. It is clear that capillary condensation cannot occur in pores of molecular dimensions and that a different pore-filling process is responsible for pore filling at very low relative pressure [38]. However, when the micropore width is greater than a few molecular diameters, the pore filling mechanism is more complex and less easy to identify.

It is now generally agreed that the filling of a very narrow pore is due to the overlap of adsorption forces across the pore. The theoretical treatment of Everett and Powl [39] confirmed earlier work [40], which had indicated that for a given gas–solid system the strongest adsorbent–adsorbate interaction is attained when the adsorptive molecules enter pores of only slightly larger width than the molecular diameter. Furthermore, the calculated energy of adsorption was estimated to be much greater in a cylindrical pore than in a slit of the same width. In the ideal case of a parallel-sided slit, the maximum enhancement of adsorption energy over that on the corresponding open surface was calculated to be about two-fold [39]. In fact, this assessment agrees well with the experimental findings for the micropore filling by argon and nitrogen [41] at 77 K and also, at much higher temperatures, for a series of *n*-alkanes [42]. In both investigations, several well-defined carbon molecular sieves were used as the microporous adsorbents.

The theoretical calculations [39] have predicted that the overlap of adsorption forces becomes very small as the pore width is increased beyond a certain distance, which in a slit-shaped pore is equivalent to about two molecular diameters [5, 39]. This estimate is also consistent with a number of experimental observations [41–43] indicating that there are two distinctive mechanisms of micropore filling. Many years ago, Brunauer [44] used the term ''ultramicropore'' to designate the pores of molecular size and later Dubinin [45] referred to the wider micropores as ''supermicropores''. Unfortunately, some confusion has subsequently arisen through the application of these terms to highly heterogeneous pore structures. In order to make further progress, it was recommended by IUPAC [10] that it is more useful to focus attention on the mechanisms of micropore filling rather than to attempt to refine the size limits of the various groups of micropores.

As we have seen, the filling of the narrowest micropores (i.e. of width equivalent to no more than two or three molecular diameters) involves enhancement of the adsorbent–adsorbate interactions and takes place at low relative pressures (at $p/p^0 < 0.01$). This process has been termed ''primary micropore filling'' and is generally associated with a significant distortion of the isotherm shape [46]. Filling of the wider micropores may occurs over a much wider range of relative pressure ($p/p^0 \approx 0.01$–0.2). The enhancement of the adsorbent–adsorbate interaction energy in the pore center is now very small and

References see page 736

the increased adsorption (quasi-multilayer adsorption) is mainly due to cooperative adsorbate–adsorbate interactions. With some systems, this is manifested in the form of an increase in the differential energy of adsorption at high fractional pore filling [47].

If the physisorption isotherm is of Type I (Fig. 1), with a plateau which is virtually horizontal, the limiting uptake may be taken as a simple measure of the micropore capacity, n_p, with respect to the adsorption of a particular gas at a stated temperature. In practice, the plateau is rarely horizontal since most microporous adsorbents have appreciable external surface areas and many also have pores in the mesopore range. The interpretation is even more complicated if there is any change in the structure of the adsorbent or the adsorbate.

To convert n_p into the micropore volume V_p, it is usually assumed that the pores are filled with the liquid adsorptive – as in the case of mesopore filling. This assumption is known as the Gurvich rule [5]. However, this does not allow for the fact that the degree of molecular packing in small pores is dependent on both pore size and pore shape [48]. This problem has been addressed by applying, for instance, microscopic methods based on statistical mechanics [e.g. molecular simulation or non-local density functional theory (NLDFT)], which allows one to describe the configuration of adsorbed molecules on a molecular level. The degree of molecular packing is then reflected in the details of the density profile.

A number of different methods have been proposed for the analysis of physisorption isotherms given by microporous solids. The main objective of much of this work was to evaluate the micropore volumes and the internal and external surface areas. The relative merits of these procedures are still under discussion and in this short review it is only possible to draw attention to some of the most popular methods and the more important recent developments.

D Micropore Analysis: Dubinin's Theory of Micropore Filling Dubinin was responsible for much of the early work on micropore filling [49]. His approach was based on the Polanyi concept of a temperature-invariant "characteristic curve" for a given adsorbent. In 1947, Dubinin and Radushkevich [50] proposed a general equation for fractional micropore filling, n/n_p, in the form

$$\frac{n}{n_p} = \exp\left[-\left(\frac{A}{\beta E_0}\right)^2\right] \tag{13}$$

where A is the Polanyi expression for the "adsorption potential":

$$A = -RT \ln\left(\frac{p}{p^0}\right) \tag{14}$$

E_0 is the "characteristic energy" for a standard vapor (usually benzene) and β is a "similarity coefficient" (i.e. a scaling factor).

In their work on the adsorptive properties of many active carbons, Dubinin and co-workers [44, 45, 49] found that an extensive range of linearity was generally obtained when $\ln n$ was plotted against A^2. By combining Eqs. (13) and (14) we thus obtain the Dubinin–Radushkevich (DR) equation [50] in the form

$$n = n_p \exp\left\{-\frac{\left[RT \ln\left(\frac{p^0}{p}\right)\right]^2}{(\beta E_0)^2}\right\} \tag{15}$$

It follows that the DR plot of $\log n$ vs. $\log^2(p^0/p)$ should be linear with intercept $\log n_p$.

Although linear DR plots have been reported [44, 45] for the physisorption of various gases and vapors by microporous carbons, there are numerous examples of the linear region being restricted to a limited range of low relative pressures [5, 51]. Furthermore, zeolites are generally found to give non-linear DR plots [45, 52].

To allow for non-linearity of such DR plots, Dubinin and Astakhov [53] put forward a more general form of characteristic curve:

$$\frac{n}{n_p} = \exp\left[-\left(\frac{A}{E}\right)^m\right] \tag{16}$$

where m is an empirical parameter, which for some isotherms turns out to be dependent on both p/p^0 and T.

By assuming that the original DR equation holds only for microporous carbons with a narrow distribution of pore size, Stoeckli and co-workers [54, 55] adopted a different approach. They express the overall adsorption in terms of a series of DR contributions, each corresponding to the filling of an individual group of pores. This extended Dubinin (or DRS) approach has been applied to a variety of simple gases on a wide range of activated carbons and the degree of heterogeneity of the micropore structure has been characterized [55]. However, the viability of this elegant approach rests on the assumption that the DR equation is applicable to each pore group and that there are no other complicating factors such as differences in surface heterogeneity.

E Micropore Analysis: Empirical Methods The first empirical method to be used as a routine procedure was the t-method of Lippens and de Boer [20]. In the original method, the amount of nitrogen adsorbed at 77 K was plotted against t, the corresponding multilayer thickness calculated from a "universal" nitrogen isotherm. It soon became evident that the use of a single multilayer

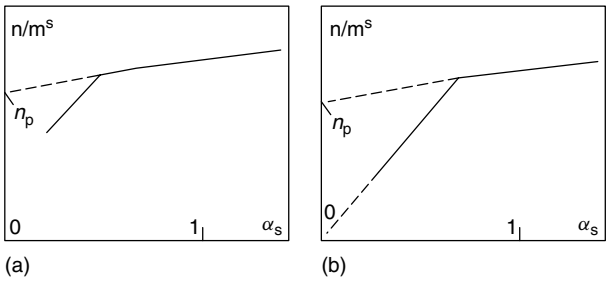

Fig. 4 Two examples of α_S plots.

isotherm is unsatisfactory and that it is necessary to determine standard isotherms on non-porous reference solids of known surface structure [5]. In addition, for the assessment of microporosity, it was suggested [5] that t should be replaced by the "reduced" adsorption, α_S – as previously defined.

The α_S method has been used for the analysis of isotherms of nitrogen, argon and alkanes [41, 42] determined on a wide range of microporous adsorbents [5, 57, 58]. The hypothetical α_S plots in Fig. 4 are typical of many experimental results and illustrate the difference in the characteristic features associated with primary and cooperative micropore filling. Primary micropore filling leads to distortion of the isotherm shape at very low relative pressure and, hence, to the appearance of the very steep initial part of the α_S plot [curve (a)]. In contrast, cooperative micropore filling takes place over a range of higher relative pressures and now there is little, if any, distortion of the initial region [as in curve (b)]. In this case, it may be supposed that the pore filling is preceded by monolayer adsorption on the pore walls – but keeping in mind that the monolayer may not be in a close-packed state. An important consequence of this difference in behavior is that it provides an approximate value of the *internal* surface area [42] from the initial slope of plot (b) but not from plot (a). If there is no detectable capillary condensation in narrow macropores, the α_S plot is linear in the multilayer region and its slope then provides a measure of the *external* surface area [5].

The micropore capacity, n_p, is the intercept on the n axis obtained by back-extrapolation of the linear multilayer section of the α_S plot [5]. Obviously, the evaluation of n_p becomes more difficult and less accurate if the external area is small or the distribution of pore size extends into the mesopore range.

Kenny et al. [38] and Kaneko et al. [59] employed high-resolution α_S analysis, which is based on the use of standard isotherm data determined at very low relative pressures so that the nitrogen α_S plots could be constructed in the primary micropore region below $\alpha_S = 0.4$. A number of comparisons have been made between the corresponding values of V_p (via n_p) obtained by application of DR and α_S methods (e.g. [41, 52, 60, 61]). Good agreement is obtained provided that the micropore filling is confined to the primary range.

The value of using adsorption calorimetry alongside isotherm measurements has been demonstrated by Fernandez-Colinas et al. [61]. A study was made of the changes in pore structure produced by the progressive activation of charcoal and the work involved an investigation of the low-temperature adsorption of argon and nitrogen. Analysis of the α_S plots provided clear evidence for the two stages of micropore filling and this was confirmed by the stepwise variation of differential enthalpy of adsorption for both Ar and N_2. It was concluded that the two methods provided consistent results, although the application of the DR method was less straightforward.

The preadsorption method [5] is another experimental technique for the determination of micropore volume. The method involves filling the micropores with large molecules (e.g. *n*-nonane), which are not removed by outgassing the adsorbent at ambient temperature. In the most straightforward case, this treatment provides a means of isolating the micropores while leaving the mesopores and open surface available for the adsorption of N_2 at 77 K. However, the preadsorbed molecules can also block pore entrances and therefore interpretation of the results is often difficult, but the method has the potential to be used to study pore blocking and network effects in porous catalysts [62].

F Other Methods for Micropore Pore Size Analysis The method of Horvath and Kawazoe (HK) [63] accounts for the enhancement of the adsorption potential as the pore size decreases. This method entails the use of high-resolution adsorption measurements at very low relative pressures.

The HK method is based on the work of Everett and Powl [64], which is a fundamental statistical analysis of a fluid confined to a slit-pore (e.g. applicable to carbon molecular sieves and other active carbons). An extension of the HK method for cylindrical pore geometry (e.g. applicable to some zeolites) was made by Saito and Foley (SF) [65] and for a spherical pore model by Cheng and Yang (CY) [66]. The spherical pore model is more suitable for cavity-type zeolites (e.g. faujasite) whereas the cylindrical pore model is justified for channel type zeolites (e.g. ZSM-5).

The HK, SF and CY methods have an advantage against the classical methods of micropore analysis (e.g. the DR method) since they are specific with respect to the pore shape and the adsorbate–adsorbent interaction potential. However, these methods neglect the real highly

References see page 736

inhomogeneous distribution of adsorbed molecules in micropores and cannot (despite improvements [67]) compete with the DFT and molecular simulation methods that are currently available.

In view of the uncertainties involved in the interpretation of adsorption isotherms, it is advisable to use different adsorptives for the characterization of microporous solids. The most direct approach is to employ a selection of molecular probes of different size and shape (e.g. helium, argon, propane, isobutane and neopentane). In this manner, it is possible to vary the ratio of pore width to molecular diameter and thereby explore any resulting differences in the two stages of micropore filling [46, 68]. This procedure, as illustrated by the work of Barton et al. [68], is eminently suitable for the characterization of microporous adsorbents and catalysts, but its use is evidently restricted to fairly small adsorptive molecules (of $d < \sim 0.8$ nm).

The use of nitrogen (at 77 K) and argon (at 87 K) as reference adsorptives deserves special mention. From the experimental standpoint, the characterization of ultramicroporous materials by nitrogen adsorption is difficult, because the filling of pores of diameter 0.5–1 nm appears to occur at relative pressures of 10^{-7}–10^{-5}, where the rates of diffusion and adsorption are very slow. The filling relative pressures of argon are 1–2 decades higher compared with nitrogen, which helps to accelerate the diffusion and adsorption equilibration. Hence it is of advantage to analyze materials containing narrow micropores by using argon as adsorptive at liquid argon temperature [2]. This is particularly important for microporous carbons, which often exhibit a wide distribution of pore sizes, including ultramicropores.

It has long been recognized (e.g. [69, 70]) that CO_2 adsorption at near-ambient temperatures is more efficient for accessing the ultramicroporosity. At 273 K, CO_2 is still ca. 32 K below its critical temperature and because the saturation pressure is very high (3 519 120 Pa), the relative pressure measurements necessary for the micropore analysis are achieved in the range of moderate pressures (133.3–101 308 Pa). For other reasons, helium adsorption at 4.2 K (i.e. below its critical temperature) was also suggested as a useful probe molecule for the ultramicropore analysis [72]: because helium is the smallest inert molecule, it can penetrate through narrow necks into some micropores, which are inaccessible for other adsorptives. Helium adsorption experiments at 4.2 K by Kaneko and co-workers [71, 72] on activated carbon fibers gave micropore volumes, as estimated by the DR method, greater than those obtained by N_2 adsorption at 77 K by 20–50%.

G Application of Density Functional Theory DFT [73, 74] and computer simulation (such as molecular dynamics and Monte Carlo simulation) [75] have been developed into powerful methods for the description of the physisorption and phase behavior of fluids confined in porous materials. They are the most advanced methods currently available for pore size analysis of microporous and mesoporous materials. Seaton et al. [76] were the first to apply DFT to calculate the pore size distribution in both the mesopore and micropore range. In this first attempt the so-called local version of DFT was used. Although the local DFT provides a reasonable qualitative description of adsorption in the pores, it is quantitatively inaccurate, especially in the range of narrow micropores. A significant improvement in accuracy was obtained with the introduction of non-local density functional theory (NLDFT), which was first developed for pore size analysis (of microporous carbons) by Lastoskie et al. [77] in 1993. Since then, the NLDFT method has been used in a number of laboratories (e.g. [78, 79]) and it is now commercially available for many adsorbent–adsorptive systems.

NLDFT describes the configuration of adsorbed molecules in pores on a molecular level and thus provides detailed information about the local fluid structure near curved solid walls as compared with the bulk fluid. It is generally assumed that in an experimental system the adsorbate in a pore is in thermodynamic equilibrium with a bulk gas phase. The local density $\rho(r)$ of the pore fluid is therefore determined by minimizing of the grand thermodynamic potential, which depends on the adopted intermolecular potentials of fluid–fluid (adsorbate–adsorbate) and fluid–solid (adsorbate–adsorbent) interactions. Once $\rho(r)$ is known, other thermodynamic properties, such as the adsorption isotherm, the energetics of adsorption and phase transitions, can be calculated.

The fluid–solid interaction potential is dependent on the pore model. In order to describe adsorption in activated carbon samples, slit-pore geometry is generally assumed [78, 79]. Other pore shape models and their appropriate potentials have been adopted, including cylindrical and spherical geometries, which are more applicable to some well-defined structures (e.g. zeolites, MCM-41, SBA-16) [79].

The parameters of the fluid–fluid interactions are usually cross-checked against the bulk properties (e.g. surface tension, gas–liquid coexistence curve). The corresponding parameters of the solid–fluid interactions can then be obtained by fitting the calculated adsorption isotherms on a planar surface to the standard (e.g. nitrogen) isotherm. In addition, it is assumed that the fluid is contained in individual pores of simple geometry (e.g. slits, cylinders or spheres). For instance, an individual slit pore in carbon can be represented as two infinite, parallel graphitic slabs. In this representation, it is customary to define the pore width, W, as the distance between the centers of surface atoms on the opposite pore walls.

Thus, NLDFT allows one to calculate for a particular adsorptive–adsorbent pair a series of theoretical isotherms, $N(p/p^0, W)$, in pores of different widths for a given pore shape. The series of theoretical isotherms is called the kernel.

The calculation of the pore size distribution function $f(W)$ is based on a solution of the general adsorption isotherm (GAI) equation [80], which correlates the experimental adsorption isotherm $N(p/p^0)$ (either adsorption or desorption branch in the case of hysteresis) with the kernel of theoretical adsorption or desorption isotherms $N(p/p^0, W)$. The GAI equation is given as

$$N\left(\frac{p}{p^0}\right) = \int_{w_{\min}}^{w_{\max}} N\left(\frac{p}{p^0}, W\right) \mathrm{f}(W)\, \mathrm{d}W \qquad (17)$$

In general, the solution of the GAI equation with respect to the pore size distribution function f(W) represents an ill-posed numerical problem. However, meaningful and stable solutions can be obtained by using regularization algorithms (e.g. [79]).

3.1.1.3 Adsorption at the Liquid–Solid Interface

3.1.1.3.1 Adsorption from Solution Adsorption at the solution–solid interface is evidently of great industrial importance and on a routine basis adsorption from solution has been used for many years for characterizing certain porous materials such as activated carbons. Although not always easy to interpret, solution adsorption measurements are of particular value when the adsorbent cannot be outgassed or for investigating molecular sieving. A detailed review (including up-to-date references) of the theoretical background and the experimental techniques for measuring adsorption from solution is given in Ref. [6].

A rigorous thermodynamic treatment of the experimental data is necessarily somewhat complex [81] because the solute and solvent are both adsorbed at the liquid–solid interface. Nevertheless, it is possible to use a solute that is preferentially adsorbed and covers virtually all of the surface at low concentration. In this case, the determination of solute adsorption is straightforward and the data are presented in the form of a specific reduced surface excess isotherm (expressed in either millimoles or milligrams of solute adsorbed per gram).

The experimental measurements are obviously facilitated if an instrumental technique (e.g. UV or IR spectroscopy) can be used to follow the change in solute concentration. It is not always easy to achieve high accuracy and a number of practical considerations and precautions must be taken into account [81]. The traditional experimental method (i.e. the *standard immersion method*) is to add a known mass of the adsorbent to a measured amount of the solution of known concentration. The container is sealed, held at constant temperature and subjected to some form of agitation (preferably tumbling); samples of the supernatant liquid are then withdrawn and analyzed. It is often difficult to establish whether equilibrium has been attained and the procedure is laborious since a fresh sample is required for the determination of each point on the adsorption isotherm.

A more elegant approach is to circulate the solution through a bed of adsorbent and monitor the concentration continuously (e.g. by passage through a UV cell): the changes in concentration can be detected by the same methods as those used in the immersion method, but they are now located on-line. This technique has a number of important advantages, including the ease of thermostating the adsorbent and adjusting the concentration. However, it is necessary to use a solid of adequate grain size (say, above 20 μm) and of sufficient mechanical strength to prevent loss of material during the experiment. These conditions are normally satisfied with most grades of inorganic catalysts such as oxides or zeolites. Whichever technique is used, care is required in controlling the experimental conditions and in particular the purity of the solvent.

Although solution–solid adsorption systems have been found to give a variety of isotherm types, many exhibit the characteristic Type I shape (see Fig. 1), with the equilibrium concentration, C_a, replacing p/p^0. In these cases, over a limited range of C_a it is generally possible to apply an empirical equation of Langmuir form:

$$\frac{n}{n_L} = \frac{bC_a}{(1 + bC_a)} \qquad (18)$$

where n is the amount of solute adsorbed at C_a, n_L is the amount adsorbed at the plateau and b is an empirical constant.

The similarity of the Type I shape is misleading because the mechanisms involved in solution–solid adsorption and gas–solid physisorption are likely to be completely different. As already indicated, a Type I isotherm for gaseous physisorption is normally associated with micropore filling. In contrast, the plateau of a Type I solute isotherm usually corresponds to monolayer completion, which is qualitatively in accordance with the classical Langmuir picture. However, there are a number of reasons why this simple interpretation does not always provide a reliable assessment of the overall surface area of a catalyst or support. Catalyst surfaces are generally heterogeneous and the effective molecular area of the solute is likely to depend on the chemical nature of the exposed sites. Furthermore, the structure of

References see page 736

the adsorbed phase may depend on the interaction (e.g. hydrogen bonding) between the adsorbed molecules or the incorporation of solvent molecules.

The role of the solvent was demonstrated by de Boer et al. [82]. In their study of the adsorption of lauric acid on activated alumina, it was found that solvent competition was most pronounced with diethyl ether, rather less so with benzene and to a negligible extent with pentane. In the last case, the plateau of the lauric acid isotherm extended over a wide range of concentration. This type of isotherm is associated with high adsorption affinity and is generally due to relatively strong adsorbent–adsorbate interactions. However, the solute monolayer is unlikely to be in a close-packed state, the molecular area being dependent on the surface chemistry. Similarly, it has been found [5] that the apparent molecular area of the adsorbed dye molecules is not constant from one type of surface to another.

Few attempts have been made to investigate the influence of porosity on adsorption from solution. A few measurements made with such solutes as iodine [83] or salicylic acid [84] have revealed that it is possible to use solute adsorption to evaluate both the micropore volume and the external surface area. The analysis of the adsorption data is conveniently made by an extension of the α_S method. Nevertheless, more work is required to establish the mechanisms involved.

3.1.1.3.2 **Heat of Immersion** The heat of immersion (or heat of wetting) is defined as the amount of heat evolved when a known mass of outgassed solid is completely immersed, but not dissolved, in a given liquid. When determined under conditions of constant temperature and pressure it becomes an enthalpy of immersion, $-\Delta H_{\text{imm}}$, which in turn is directly related to the integral enthalpy of adsorption for the equivalent gas–solid system [85]. Any change in the surface area, surface chemistry or microporosity will result in a change in the energy of immersion. Accordingly, if applied properly immersion calorimetry can be used in the following ways for the characterization of powders or porous materials: for the evaluation of the wettability, for the determination of surface polarity and site-energy distribution and for the assessment of microporosity and surface area. A comprehensive review concerning the experimental and theoretical background of these applications is given in Ref. [6]. Here, we describe only a few aspects concerning the heat of immersion and its application.

In the absence of complicating effects such as micropore filling, the magnitude of ΔH_{imm} is dependent on the nature of the liquid–solid interactions and the extent of the available surface. Thus

$$\Delta H_{\text{imm}} = a_S \Delta h \tag{19}$$

where Δh is the areal enthalpy of immersion for the given liquid–solid system and a_S is the area of the liquid–solid interface.

Immersion calorimetry has been found useful for the routine characterization of fine powders and porous materials such as activated carbons and oxides. The technique would appear to provide a means of determining a_S by a single measurement – provided that Δh is known for the liquid–solid system. If the surface area of the solid sample is at least 10 m^2, the amount of heat released is not difficult to measure with the aid of a modern calorimeter. However, the recorded heats are of scientific value only if the measurements are made under carefully controlled conditions and the changes of state are clearly defined [84].

In the early work, it was assumed that the areal enthalpy of immersion in a given liquid was almost independent of the nature of the solid surface. Later, it became apparent that the chemical nature of the surface had a part to play and also that the presence of microporosity led to enhancement of the enthalpy of immersion (in a similar manner to the enhancement of the differential enthalpy of gas adsorption). However, it turns out that the enhancement is mainly due to the increase in surface associated with the close proximity of the pore walls and that the characteristic value of Δh remains almost unchanged for a given liquid–solid system. This has been demonstrated by enthalpy of immersion measurements with activated carbons in a range of pure organic liquids (benzene, methanol, 2-propanol, cyclohexane, *tert*-butanol, α-pinene) [56]. In this work, it was found that the enthalpy of immersion was practically proportional to the surface area accessible to the liquid – including the area within the micropores. This approach provides a means of determining the total surface area of a microporous solid provided that a non-microporous standard of similar surface composition and known area is available for comparison.

A remarkable attempt was made over 50 years ago by Harkins and Jura [86] to solve the problem associated with differences in surface composition and structure. The idea was to coat the solid surface with a multilayer thick enough to have a liquid-like surface. The heat of immersion of the precoated solid was then measured. These measurements appeared to indicate that 5–7 molecular layers were required to overcome the influence of the solid surface. This layer thickness introduces a serious problem, however, since capillary condensation usually occurs at the required high relative pressure. A more recent investigation [87] has shown that this difficulty can be overcome if water is used as the wetting liquid, since two molecular layers are generally sufficient to screen the adsorbent surface. In combination with gas

adsorption, the modified Harkins–Jura method becomes a powerful tool for catalyst characterization.

3.1.1.4 Mercury Porosimetry

Mercury porosimetry is a widely accepted method for catalyst characterization [2, 88]. The main attraction of the technique is that it allows pore size analysis to be undertaken over a wide range of mesopore-macropore widths (routinely, from ca. 0.003 to ca. 400 μm). Mercury porosimetry is used also to determine the surface area and particle size distribution and to investigate the tortuosity, permeability, fractal dimension and compressibility of porous materials. Furthermore, the technique can provide useful information relating to the pore shape, network effects and the skeletal and bulk density [2, 88].

In contrast to capillary condensation, where the pore fluid wets the pore walls (i.e. the contact angle $<90^\circ$), mercury porosimetry describes a non-wetting situation (contact angle $>90^\circ$) and therefore pressure must be applied to force mercury into the pores. Thus, a progressive increase in hydrostatic pressure is applied to enable the mercury to enter the pores in decreasing order of width. Accordingly, there is an inverse relationship between the applied pressure p and the pore radius r_p, which in the simplest case of cylindrical pores is given by the Washburn equation [89]:

$$r_p = -\left(\frac{2\gamma}{p}\right)\cos\theta \qquad (20)$$

where γ is the surface tension and θ the contact angle.

To apply Eq. (20) for the calculation of r_p, it is necessary to insert values for γ and θ. Generally, γ is assumed to be 484 mN m^{-1}, which is the surface tension of pure mercury. If no detailed information about the contact θ is available, a value of 140° is customarily used [90].

In the application of mercury porosimetry, the volume of mercury entering the pore structure is measured as the applied pressure is gradually increased. The value v_i(Hg) at the applied pressure p_i apparently gives the cumulative volume of all available pores of radius equal to or greater than r_p, i.

With modern commercial equipment, the pressure can be increased from 0.003 to 408 MPa, corresponding to cylindrical pore radii of 200 μm down to 1.8 nm (by assuming a contact angle of 140°). Allowance must be made for the compressibility of mercury and elastic distortion of the sample cell.

Figure 5 shows two intrusion–extrusion cycles of mercury into a porous powder as a function of pressure (i.e. ln p). Region (A) corresponds to a rearrangement of particles within the powder bed, followed by intrusion of the interparticle voids (B). Filling of pores occurs in the region (C) and for some materials (reversible) compression is then possible at higher pressures (D).

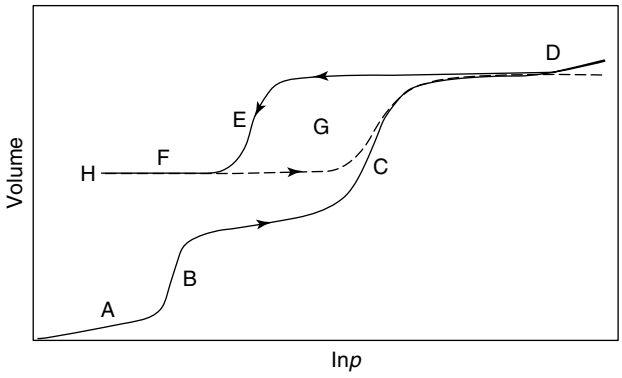

Fig. 5 Characteristic features of mercury porosimetry curves.

Hysteresis is observed and extrusion (E) occurs at different pressures than for the intrusion. On completion of a first intrusion–extrusion cycle, some mercury is always retained by the sample, thereby preventing the loop from closing (F). Intrusion–extrusion cycles after the first continue to show hysteresis (G), but eventually the loop closes, showing that there is no further entrapment of mercury. On most samples, the loop closes after just the second cycle [2, 88].

It has long been recognized [91–94] that an understanding of the hysteresis and entrapment phenomena is most important in order to be able to obtain an unambiguous mesopore size analysis, and it is not surprising that many attempts have been made to reveal the nature of these phenomena (e.g. [95–104]). Experiments with model pore networks [92] and molecular simulation studies [103, 104] appear to confirm that mercury entrapment is caused by the rupture of mercury bridges in pore constrictions during extrusion leading to mercury entrapment in ink-bottle pores. This effect is similar to that observed in a medical thermometer with decrease in temperature.

Different mechanisms have been proposed to explain intrusion–extrusion hysteresis. The single pore mechanism implies that hysteresis can be understood as an intrinsic property of the intrusion–extrusion process due to nucleation barriers associated with the formation of a vapor–liquid interface during extrusion [96] or is discussed in terms of differences in advancing and receding contact angles [97, 98]. The network models take into account the ink-bottle and percolation effects in pore networks [99–101]. It is now generally accepted that pore blocking effects, which can occur on the intrusion branch, are similar to the percolation effects involved in the desorption of gases from porous networks.

References see page 736

It is noteworthy that the shape of a mercury intrusion–extrusion hysteresis loop often agrees fairly well with that of the corresponding gas adsorption loop. Thus, the mercury intrusion and the capillary evaporation appear to follow similar pathways [102, 103]. The pore blocking–percolation effects are dominant in disordered pore networks and a reliable pore size distribution can only be calculated from the intrusion branch by applying complex network models based on percolation theory. The application of such models also allows one to obtain a limited amount of structural information from the intrusion–extrusion hysteresis loop (e.g. [95]).

In spite of its limitations, mercury porosimetry is still generally accepted as the most useful available method for the study of the macropore structure of catalysts and supports. However, it is strongly recommended that the application should not be confined to the determination of an intrusion curve alone since it is possible to identify certain distinctive features of the intrusion–extrusion behavior. Reproducibility of the hysteresis loop in a second intrusion–extrusion cycle indicates that the structure of the samples was not irreversibly affected in the first cycle (i.e. there was no fracture of the material) and gives additional information about the texture of the material. Scanning the hysteresis loop in combination with the application of advanced network models can also provide information about the pore network and the solid structure [93].

3.1.1.5 General Conclusions

The concept of surface area is universally considered to be of great practical value. However, since the textures of many catalysts and supports are exceedingly complex, no single experimental technique can be expected to provide an evaluation of the ''absolute'' surface area. Indeed, the development of fractal analysis has served to remind us of the relative nature of any specified value of specific surface area and that this quantity should always be related to the method, conditions and probe molecules used in the experimental work.

The BET-nitrogen method is still widely used for determining the surface area of mesoporous and macroporous catalysts. It is also recognized that the BET area should not be accepted as the true internal area of a microporous solid having pores of molecular dimensions (e.g. a zeolite or carbon molecular sieve). In this case, the value obtained should be regarded as an apparent or ''equivalent surface area'' and the pressure range over which the BET equation is applied should be stated. In this connection, the α_S method has been found helpful because under certain conditions it allows one to obtain an approximate estimate of both the internal and external available areas.

Important developments have allowed considerable progress to be made in nanopore size analysis. With the aid of modern computers it is now possible to apply advanced theoretical procedures. Thus, NLDFT and molecular simulation (GCMC and MD) are based on the fundamental principles of statistical mechanics as applied to the molecular behavior of confined inhomogeneous fluids. In our view, NLDFT has replaced the classical BJH method for mesopore size analysis. NLDFT has the added advantage that in principle it can be applied over the complete nanopore range. However, it is important to keep in mind that the commercially available DFT software is not strictly applicable to all types of porous materials.

We recommend the use of other probe molecules (e.g. argon adsorption at 87 K) in addition to nitrogen at 77 K for surface area determination and pore size analysis. This allows one to obtain a more accurate assessment of the mesopore size distribution. However, there are still major problems in the characterization of disordered pore structures. The interpretation of hysteresis phenomena is still under investigation, but during the last decade great progress has been made with the aid of new NLDFT-based methods. In certain cases it is now possible to obtain reliable information from both the adsorption and desorption branches of the hysteresis loop. The use of a range of probe molecules of different sizes and at different operational temperatures is advisable when characterizing microporous adsorbents. It then becomes possible to detect molecular sieving and also to identify the stages of micropore filling.

Mercury porosimetry (despite its drawbacks) remains the standard method for investigating the macropore structure of a catalyst or support. Progress has been achieved in understanding the fundamental mechanisms of pore filling so that mercury porosimetry and gas adsorption can be described within a unified theory. Further progress is likely to depend on the refinement of the theoretical principles and their application to model pore structures.

References

1. J. Haber, *Pure Appl Chem.* **1991**, *63*, 1227.
2. S. Lowell, J. Shields, M. A. Thomas, M. Thommes, *Characterization of Porous Solids and Powders: Surface Area, Pore Size and Density*, Springer-Verlag, Berlin, 2004.
3. J. Rouquerol, D. Avnir, C. W. Fairbridge, D. H. Everett, J. H. Haynes, N. Pernicone, J. D. F. Ramsay, K. S. W. Sing, K. K. Unger, *Pure Appl Chem.* **1994**, *66*, 1739.
4. K. S. W Sing, in *Handbook of Porous Solids*, F. Schüth, K. S. W. Sing, J. Weitkamp (Eds.), Vol. I, Wiley-VCH, Weinheim, 2002, p. 24.
5. S. J. Gregg, K. S. W. Sing, *Adsorption, Surface Area and Porosity*, Academic Press, London, 1982, pp. 371.
6. F. Rouquerol, J. Rouquerol, K. Sing, *Adsorption by Powders and Porous Solids*, Academic Press, London, 1999, pp. 467.

7. M. Thommes, in *Nanoporous Materials: Science and Engineering*, G. Q. Lu, X. S. Zhao (Eds.), Imperial College Press, Oxford, 2004, p. 317.
8. A. V. Neimark, in *Handbook of Porous Solids*, F. Schüth, K. S. W. Sing, J. Weitkamp (Eds.), Vol. I, Wiley-VCH, Weinheim, 2002, p. 81.
9. P. Levitz, in *Handbook of Porous Solids*, F. Schüth, K. S. W. Sing, J. Weitkamp (Eds.), Vol. I, Wiley-VCH, Weinheim, 2002, p. 37.
10. K. S. W. Sing, D. H. Everett, R. A. Haul, L. Mouscou, R. A. Pierotti, J. Rouquerol, T. Simieniewska, *Pure Appl. Chem.* **1985**, *57*, 603.
11. P. I. Ravikovitch, A. V. Neimark, *Langmuir* **2002**, *18*, 9830.
12. (a) M. Thommes, B. Smarsly, M. Groenewolt, P. I. Ravikovitch, A. Neimark, *Langmuir* **2006**, *22*, 757; (b) B. Smarsly, M. Thommes, P. I. Ravikovitch, A. V. Neimark, *Adsorption* **2005**, *11*, 653.
13. S. Brunauer, P. H. Emmett, E. Teller, *J. Am. Chem. Soc.* **1938**, *60*, 309.
14. W. A. Steele, *The Interaction of Gases with Solid Surfaces*, Pergamon Press, Oxford, 1974, p. 223.
15. P. H. Emmett, S. Brunauer, *J. Am.Chem. Soc.* **1937**, *59*, 1553.
16. A. L. McLellan, H. F Harnsberger, *J. Colloid Interface Sci.* **1967**, *23*, 577.
17. R. Rouquerol, K. S. W. Sing, in *Handbook of Heterogeneous Catalysis*, 1st ed., G. Ertl, H. Knözinger, J. Weitkamp (Eds.), Wiley-VCH, Weinheim, 1992, p. 427.
18. C. G. Shull, *J. Am. Chem. Soc.* **1948**, *70*, 1410.
19. M. R. Harris, K. S. W. Sing, *Chem. Ind. (London)* **1959**, 487.
20. J. H. Lippens, J. de Boer, *Catalysis* **1965**, *4*, 319.
21. J. de Boer, *The Dynamical Character of Adsorption*, Oxford University Press, London, 1968, p. 84.
22. K. S. W. Sing, in *Surface Area Determination*, D. H. Everett, R. H. L. Ottewill (Eds.), Butterworths, London, 1970, p. 25.
23. E. P. Barrett, L. G. Joyner, P. P. Halenda, *J. Am. Chem. Soc.* **1951**, *73*, 373.
24. L. D Gelb, K. E Gubbins, R. Radhakrishnan, M. Sliwinska-Bartkowiak, *Rep. Prog. Phys.* **1999**, *62*, 1573.
25. M. Kruk, M. Jaroniec, A. Sayari, *J. Phys. Chem. B* **1997**, *101*, 583.
26. D. H Everett, in *The Solid–Gas Interface*, E. A. Flood (Ed.), Marcel Decker, New York, 1967, p. 2.
27. (a) P. C. Ball, R. Evans, *Langmuir* **1989**, *5*, 714; (b) R. J. Evans, *J. Phys.: Condens. Matter* **1990**, *2*, 8989.
28. A. V. Neimark, P. I. Ravikovitch, A. Vishnyakov, *Phys. Rev. E* **2000**, *62*, R1493.
29. G. Mason, *J. Colloid Interface Sci.* **1982**, *88*, 36.
30. A. V. Neimark, in *Characterization of Porous Solids III*, F. Rodriguez-Reinoso, J. Rouquerol, K. S. W. Sing, K. K. Unger (Eds.), *Studies in Surface Science and Catalysis*, Vol. 62, Elsevier, Amsterdam, 1994, p. 67.
31. (a) L. Z. Zhang, N. A. Seaton, *Langmuir*, **1993**, *9*, 2576; (b) H. Liu, N. A. Seaton, *Chem. Eng. Sci.* **1994**, *49*, 1869.
32. F. Rojas, I. Kornhauser, C. Felipe, J. M. Esparza, S. Cordero, A. Dominguez, J. L. Riccardo, *Phys. Chem. Chem. Phys.* **2002**, *4*, 2346.
33. (a) L. Sarkisov, P. Monson, in *Characterization of Porous Solids V*, K. K. Unger, G. Kreysa, J. P. Baselt (Eds.), *Studies in Surface Science and Catalysis*, Vol. 128, Elsevier, Amsterdam, 2000, p. 21; (b) L. Sarkisov, P. A. Monson, *Langmuir* **2001**, *17*, 7600.
34. A. Vishnyakov, A. V. Neimark, *Langmuir* **2003**, *19*, 3240.
35. A. Schreiber, S. Reinhard, G. H. Findenegg, in *Characterization of Porous Solids VI*, F. Rodriguez-Reinoso, B. MacEnaney, J. Rouquerol, K. K. Unger (Eds.), *Studies in Surface Science and Catalysis*, Vol. 144, Elsevier, Amsterdam, 2002, p. 177.
36. (a) A. V. Neimark, *Langmuir* **1995**, *11*, 4183; (b) A. V. Neimark, P. I. Ravikovitch, M. Grün, F. Schüth, K. K. Unger, *J. Colloid Interface Sci.* **1998**, *207*, 159; (c) A. V. Neimark, P. I. Ravikovitch, *Microporous Mesoporous Mater.* **2001**, *44*, 697; (d) A. V. Neimark, P. I. Ravikovitch, A. Vishnyakov, *J. Phys.: Condens. Matter* **2003**, *1*, 347.
37. A. V. Neimark, P. I. Ravikovitch, *Microporous Mesoporous Mater.* **2001**, *44*, 697.
38. M. Kenny, K. S. W. Sing, C. Theocharis, in *Fundamentals of Adsorption, Proceedings of the Fourth International Conference on Fundamentals of Adsorption*, M. Suzuki (Ed.), Kodansha, Kyoto, 1993, p. 323.
39. D. H. Everett, J. C. Powl, *J. Chem. Soc.* **1976**, 619.
40. S. Gurfein, D. P. Dobychin, L. S. Koplienko, *Russ. J. Phys. Chem.* **1970**, *44*, 411.
41. D. Atkinson, P. J. M. Carrott, Y. Grillet, J. Rouquerol, K. S. W. Sing, in *Fundamentals of Adsorption*, A. I. Liapis (Ed.), Engineering Foundation, New York, 1987, p. 89.
42. P. J. M. Carrott, K. S. W. Sing, *J. Chromatogr.* **1987**, *406*, 139.
43. M. M. Dubinin, in *Characterization of Porous Solids*, S. J. Gregg, K. S. W. Sing, H. F. Stoeckli (Eds.), Society for Chemical Industry, London, 1979, p. 1.
44. S. Brunauer, in *Surface Area Determination*, D. H. Everett, R. H. L. Ottewill (Eds.), Butterworths, London, 1970, p. 80.
45. M. M. Dubinin, *Prog. Surf. Membr. Sci.* **1975**, *9*, 1.
46. P. J. M. Carrott, K. S. W. Sing, in *Characterization of Porous Solids I*, K. K. Unger, J. Rouquerol, K. S. W. Sing, M. Kral (Eds.), *Studies in Surface Science and Catalysis*, Vol. 39, Elsevier, Amsterdam, 1988, p. 77.
47. F. Rouquerol, S. Partyka, J. Rouquerol, in *Thermochimie*, M. Laffitte (Ed.), Editions du CNRS, Paris, 1972, p. 547.
48. P. J. M. Carrott, R. A. Roberts, K. S. W. Sing, *Chem. Ind. (London)* **1987**, 555.
49. M. M. Dubinin, *Chem. Rev.* **1960**, *60*, 235.
50. M. M. Dubinin, L. V. Radushkevitch, *Dokl. Akad. Nauk SSSR* **1947**, *55*, 331.
51. M. M. Dubinin, *Carbon* **1989**, *27*, 457.
52. P. J. M. Carrott, R. A. Roberts, K. S. W. Sing, *Carbon* **1987**, *25*, 59.
53. M. M. Dubinin, V. A. Astakhov, *Adv. Chem. Ser.* **1971**, *102*, 69.
54. H. F. Stoeckli, J. P. Houriet, A. Perret, U. Huber, in *Characterization of Porous Solids*, S. J. Gregg, K. S. W. Sing, H. F. Stoeckli (Eds.), Society for Chemical Industry, London, 1979, p. 31.
55. R. C. Bansai, J. B. Donnet, H. F. Stoeckli, *Active Carbon*, Marcel Dekker, New York, 1988, p. 141.
56. R. Denoyel, J. Fernandez-Colinas, Y. Grillet, J. Rouquerol, *Langmuir* **1993**, *9*, 5.
57. D. A. Payne, K. S. W. Sing, D. H. Turk, *J. Colloid Interface Sci.* **1973**, *43*, 287.
58. K. S. W. Sing, *Colloids Surf.* **1989**, *38*, 113.
59. K. Kaneko, C. Ishii, M. Ruike, H. Kuwabara, *Carbon* **1992**, *30*, 1075.
60. F. Rodriguez-Reinoso, *Pure Appl. Chem.* **1989**, *61*, 1859.
61. J. Fernandez-Colinas, R. Denoyel, Y. Grillet, F. Rouquerol, J. Rouquerol, *Langmuir* **1989**, *5*, 1205.
62. P. J. M. Carrott, F. C. Drummond, M. B. Kenny, R. A. Roberts, K. S. W Sing, *Colloids Surf.* **1989**, *37*, 1.
63. G. Horvath, K. Kawazoe, *J. Chem. Eng. Jpn.* **1983**, *16*, 47.
64. D. H. Everett, J. C. Powl, *J. Chem. Soc.* **1976**, 619.

65. (a) A. Saito, H. C. Foley, *AIChE J.* **1991**, *37*, 429; (b) A. Saito, H. C. Foley, *Microporous Mater.* **1995**, *3*, 531.
66. L. S. Cheng, R. T. Yang, *Chem. Eng. Sci.* **1994**, *49*, 2599.
67. M. L. Lastoskie, in *Characterization of Porous Solids V*, K. K. Unger, G. Kreysa, J. P. Baselt (Eds.), *Studies in Surface Science and Catalysis*, Vol. 128, Elsevier, Amsterdam, 2000, p. 475.
68. S. S. Barton, M. J. B. Evans, B. H. Harrison, *J. Colloid Interface Sci.* **1974**, *40*, 462.
69. J. Garrido, A. Linares-Solano, J. M. Martin-Martinez, M. Molina-Sabio, F. Rodriguez-Reinoso, R. Torregosa, *Langmuir* **1987**, *3*, 76.
70. D. Cazorla-Amoros, J. Alcaniz-Monje, A. Linares-Solano, *Langmuir* **1996**, *12*, 2820.
71. (a) H. Kuwabara, T. Suzuki, K. Kaneko, *J. Chem. Soc., Faraday Trans.* **1991**, *87*, 1915; (b) K. Kaneko, N. Setoyama, T. Suzuki, H. Kuwabara, in *Fundamentals of Adsorption, Proceedings of the IVth International Conference on Fundamentals of Adsorption*, M. Suzuki (Ed.), Kodansha, Kyoto, 1993, p. 315.
72. K. Kaneko, N. Setoyama, T. Suzuki, in *Characterization of Porous Solids III*, J. Rouquerol, F. Rodriguez-Reinoso, K. S. W. Sing, K. K. Unger (Eds.), *Studies in Surface Science and Catalysis*, Vol. 87, Elsevier, Amsterdam, 1994, p. 593.
73. (a) P. I. Ravikovitch, A. V. Neimark, *Langmuir* **2000**, *16*, 2311; (b) A. Vishnyakov, P. I. Ravikovitch, A. V. Neimark, *Langmuir* **1999**, *15*, 8736.
74. (a) P. Tarazona, *Phys. Rev. A* **1985**, *31*, 2672; (b) R. Evans, U. M. B. Marcono, P. Tarazona, *Chem. Soc. Faraday Trans.* **1986**, *82*, 1763.
75. K. E. Gubbins, in *Physical Adsorption: Experiment, Theory and Application*, J. Fraissard (Ed.), Kluwer, Dordrecht, 1997, p. 65.
76. N. A. Seaton, J. R. B. Walton, N. Quirke, *Carbon* **1989**, *27*, 853.
77. C. M. Lastoskie, K. Gubbins, N. Quirke, *J. Phys. Chem.* **1993**, *97*, 4786.
78. J. P. Olivier, W. B. Conklin, M. Szombathley, in *Characterization of Porous Solids III*, J. Rouquerol, F. Rodriguez-Reinoso, K. S. W. Sing, K. K. Unger (Eds.), *Studies in Surface Science and Catalysis*, Vol. 87, Elsevier, Amsterdam, 1994, p. 81.
79. (a) A. V. Neimark, *Langmuir* **1995**, *11*, 4183; (b) P. I. Ravikovitch, S. C. O. Domhnaill, A. V. Neimark, F. Schüth, K. K. Unger, *Langmuir* **1995**, *11*, 4765; (c) P. I. Ravikovitch, A. Vishnyakov, A. V. Neimark, *Phys. Rev. E* **2001**, *64*, 0011604.
80. S. Ross, J. P. Olivier, *On Physical Adsorption*, Wiley, New York, 1964.
81. D. H. Everett, *Pure Appl. Chem.* **1986**, *58*, 967.
82. J. H. de Boer, G. M. Houben, B. C. Lippens, W. H. Meijs, W. K. A. Walgrave, *J. Catal.* **1962**, *1*, 1.
83. J. Fernandez-Colinas, R. Denoyel, J. Rouquerol, *Adsorpt. Sci. Technol.* **1989**, *6*, 18.
84. J. Fernandez-Colinas, R. Denoyel, J. Rouquerol, in *Characterization of Porous Solids II*, F. Rodriguez-Reinoso, J. Rouquerol, K. S. W. Sing, K. K. Unger (Eds.), *Studies in Surface Science and Catalysis*, Vol. 62, Elsevier, Amsterdam, 1991, p. 399.
85. C. Letoquart, F, Rouquerol, J. Rouquerol, *J. Chem. Phys.* **1973**, *70*, 559.
86. W. D. Harkins, G. Jura, *J. Am. Chem. Soc.* **1944**, *66*, 1362.
87. S. Partyka, F. Rouquerol, J. Rouquerol, *J. Colloid Interface Sci.* **1979**, *68*, 21.
88. C. A. León y León, *Adv. Colloid Interface Sci.* **1998**, *76*, 341.
89. E. W. Washburn, *Proc. Natl. Acad. Sci. USA* **1921**, *7*, 115.
90. *Pore Size Distribution and Porosity of Solid Materials by Mercury Porosimetry and Gas Adsorption – Part 2: Analysis of Macropores by Mercury Porosimetry*, ISO 15901-1.
91. (a) L. M Pismen, *Dokl. Akad. Nauk SSSR* **1973**, *211*, 1398; (b) A. V. Neimark, *Colloid J. USSR* **1984**, *46*, 639.
92. C. D. Tsakiroglou, A. C. Payatakes, *Adv. Colloid Interface Sci.* **1998**, *75*, 215.
93. A. V. Neimark, *Colloid J. USSR* **1985**, *47*, 67.
94. L. Moscou, S. Lub, *Powder Technol.* **1981**, *29*, 45.
95. S. Rigby, in *Characterization of Porous Solids VI*, F. Rodriguez-Reinoso, B. MacEnaney, J. Rouquerol, K. K. Unger (Eds.), *Studies in Surface Science and Catalysis*, Vol. 144, Elsevier, Amsterdam, 2002, p. 185.
96. H. Giesche, *Mater. Res. Soc. Symp. Proc.* **1996**, *431*, 151.
97. (a) S. Lowell, J. E. Shields, *J. Colloid. Interface Sci.* **1981**, *80*, 192; (b) S. Lowell, J. E. Shields, *J. Colloid. Interface Sci.* **1981**, *83*, 273.
98. G. Salmas, G. J. Androutsopolous, *J. Colloid Interface Sci.* **2001**, *239*, 178.
99. M. Day, I. B. Parker, J. Bell, R. Fletcher, J. Duffe, K. S. W. Sing, D. Nicholson, in *Characterization of Porous Solids III*, J. Rouquerol, F. Rodriguez-Reinoso, K. S. W. Sing, K. K. Unger (Eds.), *Studies in Surface Science and Catalysis*, Vol. 87, Elsevier, Amsterdam, 1994, p. 225.
100. G. Zgrablich, S. Mendioroz, L. Daza, J. Pajares, V. Mayagotia, F. Rojas, W. C. Conner, *Langmuir* **1991**, *7*, 779.
101. K. L. Murray, N. A. Seaton, M. A. Day, *Langmuir* **1999**, *15*, 8155.
102. S. Lowell, J. E. Shields, *Powder Technol.* **1981**, *29*, 225.
103. F. Porcheron, P. A. Monson, M. Thommes, *Langmuir* **2004**, *20*, 6482.
104. F. Porcheron, P. A. Monson, *Langmuir* **2005**, *21*, 3179.

3.1.2 Particle Size and Dispersion Measurements

*Gérard Bergeret and Pierre Gallezot**

3.1.2.1 Definitions and Generalities

3.1.2.1.1 **Particles** In material sciences, ''particle'' is a general term for small solid objects of any size from the atomic scale (10^{-10} m) to the macroscopic scale (10^{-3} m); however, it often corresponds to the size range 10^{-9}–10^{-5} m as far as catalysts are concerned. The larger particles ($>10^{-6}$ m) are usually called grains (zeolites, carbons, Raney metals) and the smaller particles (<2 nm) are frequently called nanoparticles, aggregates (metals) or clusters (metals, oxides). The term crystallite describes a small single crystal; particles could be formed by one or more crystallites. In this chapter, particles corresponding to the active phases (metals, oxides, sulfides), rather than to the catalyst supports, will be considered and emphasis will be placed on metal particles.

* Corresponding author.